PAPER

Concentration dependent electrochemical properties and structural analysis of a simple magnesium electrolyte: magnesium bis(trifluoromethane sulfonyl)imide in diglyme†

Niya Sa,[ab] Nav Nidhi Rajput,[c] Hao Wang,[ab] Baris Key,[ab] Magali Ferrandon,[ab] Venkat Srinivasan,[c] Kristin A. Persson,[cd] Anthony K. Burrell*[ab] and John T. Vaughey*[ab]

Development of Mg electrolytes that can plate/strip Mg is not trivial and remains one of the major roadblocks to advance Mg battery research. Halogen-free electrolyte has attracted great attention due to its high stability, less corrosive nature and compatibility with Mg metal anodes. However, the electrochemical properties of such electrolytes have not been analytically evaluated in the literature. Herein, we report a systematic study of the concentration-dependent electrochemical and mass transport properties of a non-aqueous, halogen-free Mg electrolyte composed of magnesium bis(trifluoromethane sulfonyl)imide in diglyme ($Mg(TFSI)_2$/G2). Specifically, cyclic voltammograms confirm that plating and stripping of Mg in $Mg(TFSI)_2$/G2 electrolyte occur over a wide concentration range. Results suggest a comparably difficult magnesium dissolution in $Mg(TFSI)_2$/G2 electrolyte in contrast to in Grignard based electrolytes. Dissolution overpotential shows a non-monotonic dependence on electrolyte concentration, it requires an ~2 V overpotential to deposit Mg. Findings also reveal concentration-dependent mass transport properties, including concentration-dependent electrolyte diffusivity and transference number. The atomic environment of the $Mg(TFSI)_2$/G2, as being further explored by Nuclear Magnetic Resonance (NMR) measurement and Molecular Dynamics (MD) simulations, is coupled with the electrochemical measurements to explain the observed concentration-dependent mass transport properties.

1. Introduction

Rechargeable ion batteries have attracted global attention in the expansion of clean and renewable energy research. Lithium-ion batteries (LIBs) have, in fact, been the technology of choice over the past few years and have penetrated the automotive market in the format of plug-in hybrid electric vehicles and electric vehicles.[1] However, LIBs have a number of shortcomings despite their technological promise, especially with respect to battery safety, for instance, LIBs have a tendency to form dendrites at the anode, and thus cause damage of batteries operating at high voltages.[2] Beyond Li-ion batteries, for example, multivalent batteries functioning with divalent[3–7] or even trivalent ions[8] as charge carriers rather than monovalent Li ions, have been proposed as potential candidates to be alternatives for LIBs.

Mg batteries have been one of the most well-studied polyvalent-metal storage batteries owing to several merits, namely non-dendrite formation for Mg electrodeposition,[9,10] high volumetric capacity and low cost.[11] However, there are still a number of challenges for the development of Mg battery. For instance, lack of appropriate Mg electrolytes for high voltage cathodes, defined as the "roadblocks" for Mg battery development.[12] Although a number of Grignard-derived or halogen-containing electrolytes have been proposed and showed promising results for reversible Mg deposition,[13–18] application of these electrolytes are mainly limited to the low voltage Cheverl phase cathodes. On the other hand, most reported Mg electrolyte work to date, are focused on developing new synthetic strategies to achieve a better reversible Mg deposition. Majority of these electrolytes contain halogen as a component, which limits its application due to its corrosion nature.

aJoint Center for Energy Storage Research (JCESR), Argonne National Laboratory, Lemont, IL 60439, USA. E-mail: vaughey@anl.gov; burrell@anl.gov; Tel: +1-630-252-8885; +1-630-252-2629

bChemical Sciences and Engineering Division, Argonne National Laboratory, Lemont, IL 60439, USA

cEnvironmental Energy Technology Division, Lawrence Berkeley National Laboratory, Berkeley, CA 94720, USA

dDepartment of Materials Science & Engineering, University of California, Berkeley, CA 94720-1760, USA

Conventional electrolytes, for example $Mg(TFSI)_2$-based electrolytes, have attracted considerable attentions lately mainly due to its high stability and evidence of reversible Mg deposition.[19] A number of the most recent studies have shown applications of $Mg(TFSI)_2$-based electrolytes for both electrolyte development[4,19–23] and cathode applications.[24–29] However, the lack of literature on understanding the fundamental electrochemical properties of such non-halogen containing electrolyte has limited their utility as a more basic understanding of the deposition processes, and the chemistry of the solution species is required to better define their limitations and future prospects. For instance, mass transport properties such as diffusion properties, transference number of the Mg electrolytes are seldom studied or tabulated in literature. Poor mass transport in the electrolyte can potentially cause large loss of battery performance. Determination of transport properties under a near operating conditions is therefore important to investigate.

Herein, we seek to provide fundamental insights into the transport capability of the electrolyte, and therefore directly advances electrolyte design. Work presented here addresses a systematic evaluation of a concentration-dependent electrochemical properties of a $Mg(TFSI)_2$ electrolyte with an aim to answer the following questions: (1) what are the factors that govern the mass transport properties for a simple $Mg(TFSI)_2$-based electrolyte system? (2) How does the solution environment correspond to the electrochemical performance of the $Mg(TFSI)_2$ electrolyte? Yet, mass transport properties evaluated in this work provides valuable information at electrode/electrolyte interfaces to understand the electrolytic transport and its electrochemical performance.

2. Experimental materials and methods

2.1 Electrolyte preparation

Magnesium bis(trifluoromethane sulfonyl)imide was purchased from Solvionic (99.5%, Solvionic, France). The as obtained magnesium bis(trifluoromethane sulfonyl)imide was dried in a vacuum oven at 170 °C overnight before use. Diglyme (Aldrich, anhydrous, 99.5%) solvent was pretreated with molecular sieve (Aldrich, 3 Å beads, 4–8 mesh) overnight before adding into the dried $Mg(TFSI)_2$. The as-prepared electrolyte was then stirred overnight before use. Water levels of electrolytes were under 20 ppm, determined by Karl-Fischer analysis.

2.2 Electrochemical characterization

Cyclic voltammograms (CV) were determined in a home-built electrochemical cell with a Pt disk electrode (2 mm in diameter, CH instruments, Austin, TX) as working electrode, mechanically polished Mg ribbons (99.9% purity, Sigma-Aldrich) as reference and counter electrode. 1 mL of electrolyte was added into the cell for each CV measurement.

Electrochemical Impedance Spectroscopy (EIS) is applied for electrolyte conductivity measurement. A home-built conductivity cell, fabricated with two platinum disks facing each other of 1 mm separation, was used for the EIS measurement.

Conductivity cell was filled with 1 mL electrolyte with the frequency being scanned from 0.1 Hz to 100 000 Hz. Impedance is calculated according to eqn (1):

$$k = d/(A \times |\bar{z}|) \tag{1}$$

where k is ionic conductivity, d is the electrode distance, A is the area of the electrode, and $|\bar{z}|$ represents the electrolyte resistance derived from the Nyquist of the EIS measurement. Constants d and A are obtained by calibration of conductivity with standard KCl solution. All electrochemical characterizations presented in this work were carried out on a multichannel potentiostat (Parstat MC, Princetion Applied Research, TN) under a pure argon atmosphere in a glove box, where H_2O and O_2 levels are kept under 1 ppm.

2.3 Diffusion coefficient, ionic conductivity and transference number measurement

Chronocoulometry (CC) method was applied to evaluate the diffusion coefficient of electrolyte in a electrochemical cell with a Pt disk electrode (2 mm in diameter, CH instruments, Austin, TX) as working electrode, mechanically polished Mg ribbons (99.9% purity, Sigma-Aldrich) as reference and counter electrode. Potential at the working electrode was set at -0.5 V against Mg/Mg^{2+} for 120 s allowing the reduction of cations at the surface of the working electrode. All the electrochemical characterizations mentioned in this paper were carried on a multi-channel potentiostat (Parstat MC, Princetion Applied Research, TN) under pure argon atmosphere in a glove box. Integration of the faradic current density over time was obtained and plotted against the square root of time. Diffusion coefficient at each concentration was determined by fitting Q versus $t^{1/2}$ as shown in eqn (1) derived from the Cottrell equation,

$$Q = \frac{2nFAC_0 D^{1/2}}{\pi^{1/2}} t^{1/2} + Q_{dl} + Q_{ads} \tag{2}$$

Corresponding parameters of eqn (2) are defined as follows: n as the number of electrons for the reduction reaction occurred at the working electrode ($n = 2$); F is the Faraday constant; A as the electrode area (0.0314 cm^2), Q_{dl} as capacitive charge and Q_{ads} as charge contributed from the absorbed species.[30] Here, charge from Q_{dl} and Q_{ads} are not considered since it contributes less than 1% as compared to the total charge contributed from Mg plating.

Transference number is determined by quantification of the amount of potentiometric Mg deposition by atomic absorption spectroscopy (AAS), a method reported in literature.[30] A controlled amount of charge is passed between the working electrode and the reference electrode, and current carried by cations is consequently determined by AAS quantifying the concentration loss caused by electrolysis. Specifically, Mg was firstly deposited at -0.5 V vs. Mg/Mg^{2+}. The deposits were then dissolved in a 0.1 M HNO_3 solution, and this solution was analyzed through AAS (PerkinElmer, AAnalyst100 Spectrum, wavelength 285.2 nm, air/acetylene flame) to determine the

concentration loss of Mg. Transference number is then calculated through eqn (3),

$$t_+ = 1 - \left(\frac{z_+ F \Delta CV}{it} \right) \tag{3}$$

where t_+ represent transference number of cations; z_+, F, ΔC, V correspond to charge number, Faraday constant, change of bulk Mg concentration and the volume of electrolyte, respectively. Current (i) and time (t) stand for the total amount of charge passed through the cell.

2.4 SEM and EDX analysis of electrochemically deposited Mg from a Mg(TFSI)$_2$/G2 electrolyte

Morphologies of the electrochemically deposited Mg metal from Mg(TFSI)$_2$/G2 electrolytes were characterized by SEM (Quanta-400F, FEI, Hillsboro, OR) operated at a potential of 20 kV. Energy Dispersive X-ray Spectroscopy (EDX) was applied to determine the purity of the deposited Mg, at an electron energy of 30 keV. A current density of 3.6 C cm^{-2} was applied to the electrolyte for the electrochemical deposition.

2.5 NMR characterization

NMR spectra were acquired with a 300 MHz Bruker Avance spectrometer. D$_2$O was sealed in a capillary and used as an internal reference. A recycle delay of 2 s was used when acquiring ^{13}C NMR spectra, 5 s for ^{25}Mg NMR spectra and 1 s for ^{1}H NMR spectra.

2.6 Molecular dynamics simulation

Classical molecular dynamics (MD) simulations were performed using GROMACS MD simulation package version 4.5.3.[31] The initial configuration was obtained by randomly packing molecules in a cubic box with periodicity in *XYZ* directions. The bonded and non-bonded parameters are described using generalized amber force field (GAFF) while the atomic charges are derived by fitting the electrostatic potential surface using RESP methodology of molecule with geometry optimized at B3LYP/6-311++G(d, p) level using the Gaussian 09 package.[32] Details of MD simulations setup and force field have been described in our previous paper.[33]

3. Results and discussion

3.1 Concentration dependent plating and stripping magnesium in Mg(TFSI)$_2$/diglyme

To evaluate reversible Mg deposition, cyclic voltammetry (CV) is conducted in a home-built, three electrode cell with Pt disk as working electrode, polished Mg ribbons as counter and reference electrode. Fig. 1a presents CVs of Mg(TFSI)$_2$/G2 electrolyte at a concentration range from 0.1 M to 1.5 M. Results show evident current peaks for both plating and stripping of Mg. It is clear that Mg deposition is partially reversible in a wide concentration range. Deposited Mg is confirmed with SEM and EDX analysis as shown in Fig. 2, where signature spectra of Mg is clearly observed demonstrating nearly pure Mg deposition from the Mg(TFSI)$_2$/G2 electrolyte. Trace signal of elements C, O
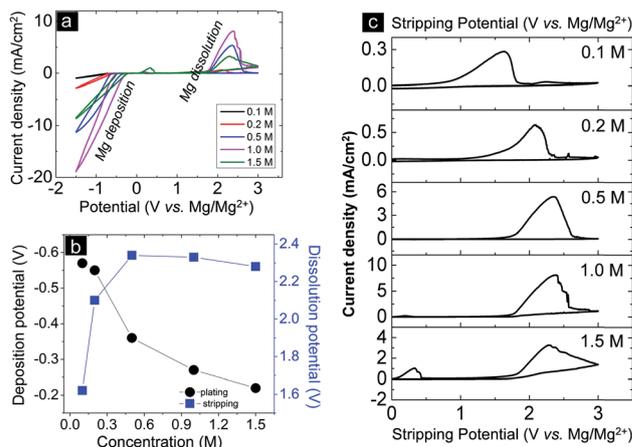

Fig. 1 (a) Cyclic voltammograms of Mg(TFSI)$_2$/G2 electrolyte at a concentration range from 0.1 M to 1.5 M; (b) concentration dependence of the Mg deposition (black)/dissolution (blue) onset potential; (c) zoomed in graph of the major stripping peak from panel a; CV is collected based on a three electrode setup, with Pt disk as working electrode and polished Mg ribbons as reference and counter electrode at scan rate of 25 mV s^{-1}.
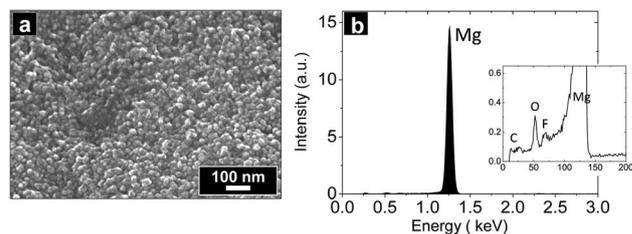

Fig. 2 (a) Scanning electron micrographs (SEM) of electrochemically deposited Mg at 3.6 C cm^{-2} from the Mg(TFSI)$_2$/G2 electrolyte; (b) energy-dispersive X-ray spectroscopy analysis of deposited Mg metal from a Mg(TFSI)$_2$/G2 electrolyte. Inset shows zoomed image at low energy.

and F can also be observed (inset of Fig. 2b), suggesting either a possible electrolyte decomposition or existence of the trace electrolyte residue at Mg surface. CV results suggest that current density of magnesium deposition and dissolution increases as electrolyte concentration increases, from 0.1 M to 1.0 M, but it decreases at the very extreme high concentration, 1.5 M. Such decay could possibly due to reduced Mg mobility or ion pair formation that lowers the total number of effective charge carriers.[33,34] Worth to note that besides the major stripping curve beyond 1 V *vs.* Mg/Mg^{2+}, an extra tiny stripping peak, ~0.4 V *vs.* Mg/Mg^{2+}, can also be seen in the CV (Fig. 1a). We believe overpotentials of the stripping curves are closely correlated to the trace water and impurity level of the electrolyte, also reported in two recent publications.[25,35]

To further evaluate the correlation of the electrolyte concentration to the electrochemical property of the Mg(TFSI)$_2$/G2 system, concentration *versus* the plating/stripping onset potential, over-potential and coulombic efficiency is plotted and listed in Fig. 1b and c and Table 1, respectively. Onset potential for Mg deposition decreases as the electrolyte concentration

Table 1 Electrochemical properties of Mg(TFSI)$_2$/G2 electrolyte at concentrations range from 0.1 M to 1.5 M

	0.1 (M)	0.2 (M)	0.5 (M)	1.0 (M)	1.5 (M)
Coulombic efficiency (%)	19	15	24	23	27
Plating potential (V)	−0.57	−0.55	−0.36	−0.27	−0.22
Stripping potential (V)	1.62	2.1	2.34	2.33	2.28
Over-potential	2.17	2.6	2.7	2.6	2.5

Fig. 3 (a) Concentration dependent ionic conductivity of Mg(TFSI)$_2$/G2 electrolyte at a concentration range from 0.1 M to 1.5 M. (b) Concentration dependent diffusion coefficient of Mg(TFSI)$_2$/G2 electrolyte at concentrations range from 0.1 M to 1.5 M. Measurements were performed at room temperature, 298 K.

increases, for instance, deposition onset potential gradually decreases from −0.57 V to −0.22 V as electrolyte concentration increases from 0.1 M and 1.5 M. On the other hand, magnesium dissolution in the Mg(TFSI)$_2$/G2 electrolyte is comparably difficult, and requires a ∼2 V higher potential than that needed to deposit Mg (Fig. 1b and c). Such over-potential can be ascribed to the formation of a surface layer at the interface of Mg(TFSI)$_2$/G2 electrolyte and Mg anode.[36–38] Stripping potential for Mg dissolution shows concentration dependence as well. It increases with increasing the Mg(TFSI)$_2$ concentration (Fig. 1c), for instance, stripping potential is 1.62 V and 2.28 V as concentration increases from 0.1 M to 1.5 M. Such observed potential difference indicates that Mg dissolution is less energetically favorable at higher electrolyte concentrations, which can be explained by the highered desolvation energy at high electrolyte concentrations and the altered nucleation energetics of Mg at a polycrystalline Pt surface.[39,40] Worth to note here, unlike the complex organomagnesium based electrolytes in ethers, which are strongly reducing and yield nearly 100% coulombic efficiency, the Mg(TFSI)$_2$/G2 electrolyte reported here has ∼30% coulombic efficiency (Table 1). We believe the diglyme solvent plays a critical factor to provide a well dissociated environment for Mg ions, and therefore to facilitate efficient Mg deposition and dissolution.

3.2 Concentration dependent ionic conductivity, diffusivity and transport number in the Mg(TFSI)$_2$/G2 electrolyte

3.2.1 Concentration dependent ionic conductivity. Ionic conductivity of electrolyte is a critical factor to affect battery cycle life. Ideally, electrolyte of high ionic conductivity is desired, since it allows battery's internal resistance to be minimized. Results of the concentration dependent ionic conductivity of Mg(TFSI)$_2$/G2 is presented in Fig. 3a. Conductivity increases with electrolyte concentration. It reaches to a peak value at 1.0 M, 5.2 mS cm^{-1}, and then decreases at the highest concentration strength of 1.5 M. The gain of conductivity from 0.1 M to 1.0 M is a good indication of the proportional ionization of Mg(TFSI)$_2$/G2 electrolyte at an increase of the total number of active ions. However, the observed conductivity decline at the extreme concentration, 1.5 M, due to a lowered ionic mobility from ion pair formation and this finding is qualitatively consistent with the previous theoretical predictions for Mg(TFSI)$_2$ electrolyte. Such phenomenon is further investigated in the following NMR discussion. Worth to note that the observed ionic conductivity is higher than most of the reported organo-halide or organomagnesium based electrolytes, where the highest ionic conductivity is ∼3 mS cm^{-1}.[3,19]
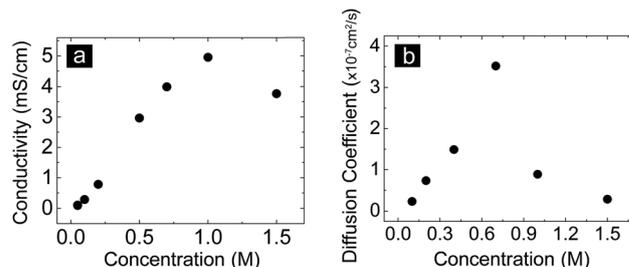
The improved ionic conductivity makes Mg(TFSI)$_2$/G2 attractive for battery application, due to the minimized internal resistance and thus a higher power density can be permitted. Recent published work have shown application of such Mg(TFSI)$_2$/G2 electrolyte for a V$_2$O$_5$ cathode based Mg battery.[24,25]

3.2.2 Correlation of ion diffusivity with electrolyte concentration. Ion diffusion in non-aqueous electrolyte provides the fundamental knowledge of understanding the mass transport property of the system. Herein, a chronocoulometry method is applied to evaluate the effect of concentration dependent cation diffusion coefficient of the Mg(TFSI)$_2$/G2 electrolyte. A negative potential (−0.5 V), where Mg deposition occurs, is applied between the Pt working electrode and the Mg reference electrode. A depletion of the cation species near the electrode, reflected by a measurement of current decay, leads to an inverse of $t^{1/2}$ function and such trend suggests a typical diffusion controlled process.[30] Diffusion coefficient at each concentration was determined by fitting Q versus $t^{1/2}$ with eqn (1) derived from the Cottrell equation.

Results suggest that the Mg(TFSI)$_2$/G2 electrolyte attains a nonlinear, complex diffusion profile *versus* electrolyte concentration, as shown in Fig. 3b. At lower electrolyte concentrations, a depletion of cation concentration at the electrode surface is observed, and is mainly due to the double layer formed at the working electrode which hinders diffusion, considering the thickness of the double layer increases with decreasing the electrolyte concentration. As concentration increases, active cations (could be Mg^{2+} or other format of cations) are diffused from the bulk electrolyte to the surface of the electrode, and as a result an increase of the faradic current is observed as suggested from the chronocoulogram. Diffusion coefficient (D_f) increases about one order of magnitude as electrolyte concentration increases from 0.1 M to 0.7 M, from 2.28×10^{-7} cm^2 s^{-1} to 3.51×10^{-6} cm^2 s^{-1}. A significant decline of diffusion coefficient is observed at an extreme high electrolyte concentration 1.5 M, and D_f decreases down to 2.8×10^{-7} cm^2 s^{-1}. Such effect could assign to the possible dimerization effect at highly concentrated electrolyte solution. A detailed NMR study is followed up to further explain the possible solvation structural of electrolyte at high concentration. The concentration dependent ion diffusion profile suggests complicated solution environment at different ionic strength, and the initial concentration of the active Mg^{2+} species could play

a crucial role to trigger different electrochemical behavior of the electrolyte. It is worth to mention that this finding is different from the reported Grignard-derived organohaloaluminate electrolyte, $C_2H_5MgCl–(C_2H_5)_2AlCl_2$, where a decrease of diffusion effect is described at increased concentration.[30]

3.2.3 Ionic transference number.

Ionic transference number, a measurement of the fraction of total current carried in an electrolyte by a given ion, is evaluated systematically for the $Mg(TFSI)_2/G2$ electrolyte in a wide concentration range. Herein, to gain insightful information of the concentration dependent electrochemical property of the $Mg(TFSI)_2/G2$ electrolyte, transference numbers (t_+) at various concentrations are measured and compared with the halogen-contained electrolytes such as $[Mg_2(–Cl)_3·6(OC_4H_8)]$[30] and the dichloro complex (DCC) electrolyte. Table 2 shows a decrease of transference number with an increase of concentration of $Mg(TFSI)_2/G2$ in both dilute and concentrated regimes. Specifically, transference number decreases from 0.297 to 0.036, about 10 folds, as electrolyte concentration increases from 0.2 M to 1.5 M. Such difference in transport number arises from the difference of ion mobility, in good agreement with the results from conductivity and diffusivity measurements. At higher concentration, coordination environment of cation species are changed. Shielding effects from anions to the active cation species containing Mg^{2+} become more prominent at higher electrolyte concentrations, and thus results in a more limited cation motion. The cation transference number of $Mg(TFSI)_2/G2$ at 0.5 M, 0.141, is quite comparable to the halogen contained electrolyte, t_+ is determined to be 0.159 and 0.13 for APC and DCC, respectively. This finding suggests dissociation of anions in electrolyte contributes and dominates to the majority of the current reading.

3.3 NMR characterization for $Mg(TFSI)_2/G2$ at high and low concentrations

The structure and the coordination environment of the $Mg(TFSI)_2/G2$ electrolyte are further studied and analyzed with NMR spectroscopy. ^{25}Mg, ^1H, ^{13}C NMR spectra were acquired for two representative concentration regimes: a low concentration electrolyte (0.1 M) and a high concentration electrolyte (1.5 M). ^{25}Mg NMR spectra show a clear line shape difference between the low (full width half maximum (FWHM) = 24.5 ppm) and high (FWHM = 8.8 ppm) concentration electrolyte, presented in Fig. 4a. The broadening of the line shape was observed for the concentrated electrolyte, and this
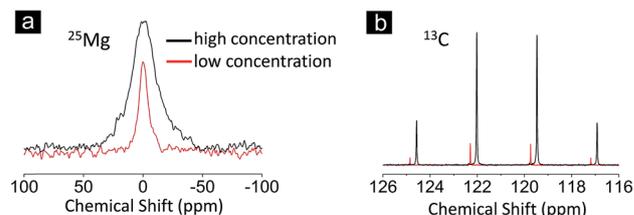
Fig. 4 NMR characterization of $Mg(TFSI)_2/G2$ electrolyte at high (black line) and low concentration (red line). (a) ^{25}Mg NMR; (b) ^{13}C NMR, in the TFSI anion.

phenomenon was ascribed to the decrease of the electrolyte/solvent mobility, due to the ion pair formation in the high concentration electrolyte, which is further discussed in detail in the Simulation section. In the diluted electrolyte (0.1 M), electrolyte molecules can move less restricted than in the concentrated electrolyte, giving a narrower ^{25}Mg NMR spectrum (red curve, Fig. 4a) than that of the concentrated electrolyte (black curve, Fig. 4a). Peak shift in Fig. 4b (^{13}C NMR spectra) was also observed, and all peaks shifted to upfield for the concentrated electrolyte suggesting an intensified shielding effect applied to the TFSI anions. In addition, the ^{13}C NMR spectrum is broadened due to the intensified $Mg^{2+}/TFSI^-$ interaction (0.05 ppm for concentrated electrolyte compared with 0.02 ppm for the diluted electrolyte). The change in the molecule environment can be explained by the increased interaction (such as ion pair formation) in a concentrated electrolyte causing changes of the peaks in NMR spectra.

3.4 Molecular dynamic simulation of $Mg(TFSI)_2/G2$ electrolyte

Molecular dynamics simulations were performed on $Mg(TFSI)_2/G2$ electrolyte systems, employing high and low concentration regimes at room temperature. Results indicate that the solution structure differs remarkably for electrolyte at dilute and concentrated solutions, as shown in Fig. 5. Number of the $TFSI^-$ anion in the first solvation shell around Mg^{2+} cation increases with increasing electrolyte concentration. At lower concentration Mg-TFSI forms solvent separated ion pairs (SSIPs) with coordination number less than 1 (ESI, Fig. S1†). At higher concentration, 1.5 M, the coordination number increases to 1.6, however, no cluster formation observed due to more dispersed charge and two large sulfonyl groups of the $TFSI^-$ anion (ESI,

Table 2 Ionic transport measurement based on electrolysis method for non-aqueous Mg electrolytes

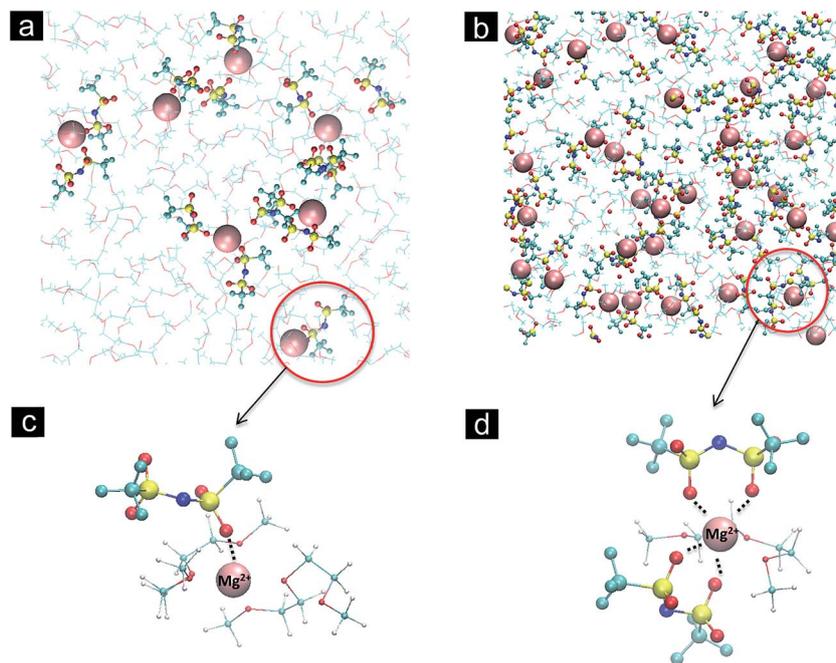| Electrolyte	Concentration (M)	Mg (ppm)	ΔC (mM)	t_+	t_-
$Mg(TFSI)_2/G2$	0.2	2.099	2.10	0.297	0.703
$Mg(TFSI)_2/G2$	0.5	2.576	2.58	0.141	0.859
$Mg(TFSI)_2/G2$	1.0	2.571	2.61	0.130	0.870
$Mg(TFSI)_2/G2$	1.5	3.297	2.90	0.036	0.964
$[Mg_2(–Cl)_3·6(OC_4H_8)]^+$ (ref. 41)	0.4	35.61	0.73	0.018	0.982
DCC/THF	0.5	2.595	2.62	0.130	0.870
APC/THF	0.5	2.478	2.53	0.159	0.841

Fig. 5 Representative simulation snapshot of (a) 0.1 M; (b) 1.5 M Mg(TFSI)$_2$/G2 at 298 K. Mg depicted in pink in space filling format, TFSI in licorice and diglyme in line format; (c) and (d) shows the zoomed image of solvation structure around an Mg ion in 0.1 M and 1.5 M concentrations, respectively.

Fig. S1†). Our previous work indicates that anions in Mg electrolytes play a significant role in determining the solvation structure and hence the solubility of Mg salts.[33] At low concentration of Mg(TFSI)$_2$, a greater number of monodentate interaction was observed between the anion TFSI$^-$ and cation Mg^{2+}, whereas at higher concentrations bidentate configuration of TFSI$^-$ anion dominates, indicated in Fig. 5. A single peak is observed in radial distribution function (RDF) corresponding to monodentate orientation of TFSI around Mg at lower concentration. Whereas, at higher concentration two peaks are observed in the RDF, where the first peak correspond to bidentate orientation and the second peak to monodentate orientation of TFSI anion (ESI, Fig. S2†). Such change in orientation of TFSI anion at higher concentration increases oxygen atom coordination with Mg ions. A recent experimental work reported by Buttry also observed more dominating bidentate configurations of TFSI$^-$ at higher concentrations.[42] It is valuable to understand the effect of solvation structure on the diffusion coefficient of ionic species in the solution. Here, we observed that the self-diffusion coefficient of both the cation and the anion gradually decreased as the Mg(TFSI)$_2$ concentration increased. At higher concentration, lack of available free volume and strong interaction between solute and solvent could results in slower dynamics of ions, in agreement with the measurement of transference number and NMR as shown in previous sections.

4.   Conclusions

A systematic evaluation of the electrochemical properties of a non-Grignard, non-halogen containing electrolyte Mg(TFSI)$_2$/

G2 is investigated both experimentally and theoretically. Electrochemical deposition of Mg, ionic conductivity, diffusion coefficient and ionic transference number were measured as a function of electrolyte concentration. Results reveal a non-linear electrochemical properties of Mg(TFSI)$_2$/G2 at diluted and concentrated regimes. For instance, dissolution overpotential increases with electrolyte concentration and decreases at an extreme electrolyte concentration, diffusion coefficient and transference number likewise shows a two polar response at diluted and concentrated regimes. Atomic environment of the electrolyte is further analyzed by Nuclear Magnetic Resonance (NMR) and MD simulations, results suggest a decrease of ionic mobility at extremely high electrolyte concentration. The change in the shielding environment at high/low electrolyte concentration between the electrolyte molecules and the solvent molecules provides insights in comprehending the observed concentration-dependent electrolyte properties. Design of future Mg electrolyte would advance with understanding and improvement of the electrolyte mass transport properties.

Conflict of interest

The authors declare no competing financial interest.

Acknowledgements

References

1 J. B. Goodenough and K.-S. Park, *J. Am. Chem. Soc.*, 2013, **135**, 1167–1176.

2 F. Orsini, A. Du Pasquier, B. Beaudoin, J. M. Tarascon, M. Trentin, N. Langenhuizen, E. De Beer and P. Notten, *J. Power Sources*, 1998, **76**, 19–29.

3 H. D. Yoo, I. Shterenberg, Y. Gofer, G. Gershinsky, N. Pour and D. Aurbach, *Energy Environ. Sci.*, 2013, **6**, 2265–2279.

4 I. Shterenberg, M. Salama, Y. Gofer, E. Levi and D. Aurbach, *MRS Bull.*, 2014, **39**, 453–460.

5 R. Mohtadi, M. Matsui, T. S. Arthur and S.-J. Hwang, *Angew. Chem., Int. Ed.*, 2012, **51**, 9780–9783.

6 G. G. Amatucci, F. Badway, A. Singhal, B. Beaudoin, G. Skandan, T. Bowmer, I. Plitza, N. Pereira, T. Chapman and R. Jaworski, *J. Electrochem. Soc.*, 2001, **148**, A940–A950.

7 D. Aurbach, Z. Lu, A. Schechter, Y. Gofer, H. Gizbar, R. Turgeman, Y. Cohen, M. Moshkovich and E. Levi, *Nature*, 2000, **407**, 724–727.

8 M.-C. Lin, M. Gong, B. Lu, Y. Wu, D.-Y. Wang, M. Guan, M. Angell, C. Chen, J. Yang, B.-J. Hwang and H. Dai, *Nature*, 2015, **520**, 324–328.

9 M. Matsui, *J. Power Sources*, 2011, **196**, 7048–7055.

10 C. Ling, D. Banerjee and M. Matsui, *Electrochim. Acta*, 2012, **76**, 270–274.

11 G. Gershinsky, H. D. Yoo, Y. Gofer and D. Aurbach, *Langmuir*, 2013, **29**, 10964–10972.

12 J. Muldoon, C. B. Bucur, A. G. Oliver, T. Sugimoto, M. Matsui, H. S. Kim, G. D. Allred, J. Zajicek and Y. Kotani, *Energy Environ. Sci.*, 2012, **5**, 5941–5950.

13 T. Liu, Y. Shao, G. Li, M. Gu, J. Hu, S. Xu, Z. Nie, X. Chen, C. Wang and J. Liu, *J. Mater. Chem. A*, 2014, **2**, 3430–3438.

14 Y. W. Cheng, T. B. Liu, Y. Y. Shao, M. H. Engelhard, J. Liu and G. S. Li, *J. Mater. Chem. A*, 2014, **2**, 2473–2477.

15 R. E. Doe, R. Han, J. Hwang, A. J. Gmitter, I. Shterenberg, H. D. Yoo, N. Pour and D. Aurbach, *Chem. Commun.*, 2014, **50**, 243–245.

16 N. Sa, B. Pan, A. Saha-Shah, A. A. Hubaud, J. T. Vaughey, L. A. Baker, C. Liao and A. K. Burrell, *ACS Appl. Mater. Interfaces*, 2016, 16002–16008.

17 T. Liu, J. T. Cox, D. Hu, X. Deng, J. Hu, M. Y. Hu, J. Xiao, Y. Shao, K. Tang and J. Liu, *Chem. Commun.*, 2015, **51**, 2312–2315.

18 B. Pan, J. Huang, N. Sa, S. M. Brombosz, J. T. Vaughey, L. Zhang, A. K. Burrell, Z. Zhang and C. Liao, *J. Electrochem. Soc.*, 2016, **163**, A1672–A1677.

19 S. Y. Ha, Y. W. Lee, S. W. Woo, B. Koo, J. S. Kim, J. Cho, K. T. Lee and N. S. Choi, *ACS Appl. Mater. Interfaces*, 2014, **6**, 4063–4073.

20 S. H. Lapidus, N. N. Rajput, X. Qu, K. W. Chapman, K. A. Persson and P. J. Chupas, *Phys. Chem. Chem. Phys.*, 2014, **16**, 21941–21945.

21 N. N. Rajput, X. Qu, N. Sa, A. K. Burrell and K. A. Persson, *J. Am. Chem. Soc.*, 2015, **137**, 3411–3420.

22 I. Shterenberg, M. Salama, H. D. Yoo, Y. Gofer, J.-B. Park, Y.-K. Sun and D. Aurbach, *J. Electrochem. Soc.*, 2015, **162**, A7118–A7128.

23 Y. Cheng, R. M. Stolley, K. S. Han, Y. Shao, B. W. Arey, N. M. Washton, K. T. Mueller, M. L. Helm, V. L. Sprenkle, J. Liu and G. Li, *Phys. Chem. Chem. Phys.*, 2015, **17**, 13307–13314.

24 N. Sa, T. L. Kinnibrugh, H. Wang, G. Sai Gautam, K. W. Chapman, J. T. Vaughey, B. Key, T. T. Fister, J. W. Freeland, D. L. Proffit, P. J. Chupas, G. Ceder, J. G. Bareno, I. D. Bloom and A. K. Burrell, *Chem. Mater.*, 2016, **28**, 2962–2969.

25 N. Sa, H. Wang, D. L. Proffit, A. L. Lipson, B. Key, M. Liu, Z. Feng, T. T. Fister, Y. Ren, C.-J. Sun, J. T. Vaughey, P. A. Fenter, K. A. Persson and A. K. Burrell, *J. Power Sources*, 2016, **323**, 44–50.

26 Z. Feng, X. Chen, L. Qiao, A. L. Lipson, T. T. Fister, L. Zeng, C. Kim, T. Yi, N. Sa, D. L. Proffit, A. K. Burrell, J. Cabana, B. J. Ingram, M. D. Biegalski, M. J. Bedzyk and P. Fenter, *ACS Appl. Mater. Interfaces*, 2015, **7**, 28438–28443.

27 J. T. Incorvati, L. W. F. Wan, B. Key, D. H. Zhou, C. Liao, L. Fuoco, M. Holland, H. Wang, D. Prendergast, K. R. Poeppelmeier and J. T. Vaughey, *Chem. Mater.*, 2016, **28**, 17–20.

28 B. Pan, D. Zhou, J. Huang, L. Zhang, A. K. Burrell, J. T. Vaughey, Z. Zhang and C. Liao, *J. Electrochem. Soc.*, 2016, **163**, A580–A583.

29 Y. Orikasa, T. Masese, Y. Koyama, T. Mori, M. Hattori, K. Yamamoto, T. Okado, Z. D. Huang, T. Minato, C. Tassel, J. Kim, Y. Kobayashi, T. Abe, H. Kageyama and Y. Uchimoto, *Sci. Rep.*, 2014, **4**, 5622.

30 A. Benmayza, M. Ramanathan, T. S. Arthur, M. Matsui, F. Mizuno, J. Guo, P.-A. Glans and J. Prakash, *J. Phys. Chem. C*, 2013, **117**, 26881–26888.

31 S. Pronk, S. Páll, R. Schulz, P. Larsson, P. Bjelkmar, R. Apostolov, M. R. Shirts, J. C. Smith, P. M. Kasson, D. van der Spoel, B. Hess and E. Lindahl, *Bioinformatics*, 2013, 845–854.

32 M. Frisch, G. Trucks, H. Schlegel, G. Scuseria, M. Robb, J. Cheeseman, G. Scalmani, V. Barone, B. Mennucci and G. Petersson, *B01*, Gaussian Inc., Wallingford CT, 2009.

33 N. N. Rajput, X. Qu, N. Sa, A. K. Burrell and K. A. Persson, *J. Am. Chem. Soc.*, 2015, 3411–3420.

34 D. K. Lee and H. R. Allcock, *Solid State Ionics*, 2010, **181**, 1721–1726.

35 J. G. Connell, B. Genorio, P. P. Lopes, D. Strmcnik, V. R. Stamenkovic and N. M. Markovic, *Chem. Mater.*, 2016, 8268–8277.

36 B. V. Ratnakumar, *J. Appl. Electrochem.*, 1988, **18**, 268–279.

37 Z. Lu, A. Schechter, M. Moshkovich and D. Aurbach, *J. Electroanal. Chem.*, 1999, **466**, 203–217.

38 R. Mohtadi and F. Mizuno, *Beilstein J. Nanotechnol.*, 2014, **5**, 1291–1311.

39 D. W. McOwen, D. M. Seo, O. Borodin, J. Vatamanu, P. D. Boyle and W. A. Henderson, *Energy Environ. Sci.*, 2014, **7**, 416–426.

40 K. Yoshida, M. Nakamura, Y. Kazue, N. Tachikawa, S. Tsuzuki, S. Seki, K. Dokko and M. Watanabe, *J. Am. Chem. Soc.*, 2011, **133**, 13121–13129.

41 A. Benmayza, M. Ramanathan, T. S. Arthur, M. Matsui, F. Mizuno, J. Guo, P.-A. Glans and J. Prakash, *J. Phys. Chem. C*, 2013, **117**, 26881–26888.

42 T. Watkins and D. A. Buttry, *J. Phys. Chem. B*, 2015, **119**, 7003–7014.